Supporting Information

Atomic Layer Deposition Fabricated Core-shell Nanostructures for Enhanced Polyetherimide Composite Dielectrics

Xudong Wu [a,b], Guanghui Song [a,c], Wangle Zhang [d], Hao Feng [d], Yichen Liu [a], Enling Huang [a], Xiaotian Lin [a], Yixin Yang [a,b], Daniel Q. Tan [a,c] *

[a] Department of Materials Science and Engineering, Guangdong Technion Israel Institute of Technology, 241 Daxue Road, Shantou, 515063, P. R. China.

[b] Department of Materials Science and Engineering, Technion - Israel Institute of Technology, Haifa 3200003, Israel.

[c] Guangdong Provincial Key Laboratory of Materials and Technology for Energy Conversion, 241 Daxue Road, Shantou 515063, PR China.

[d] Xi'an Modern Chemistry Institute, Xi'an, 710065, China

*Corresponding author: Daniel Q. Tan

E-mail: daniel.tan@gtiit.edu.cn

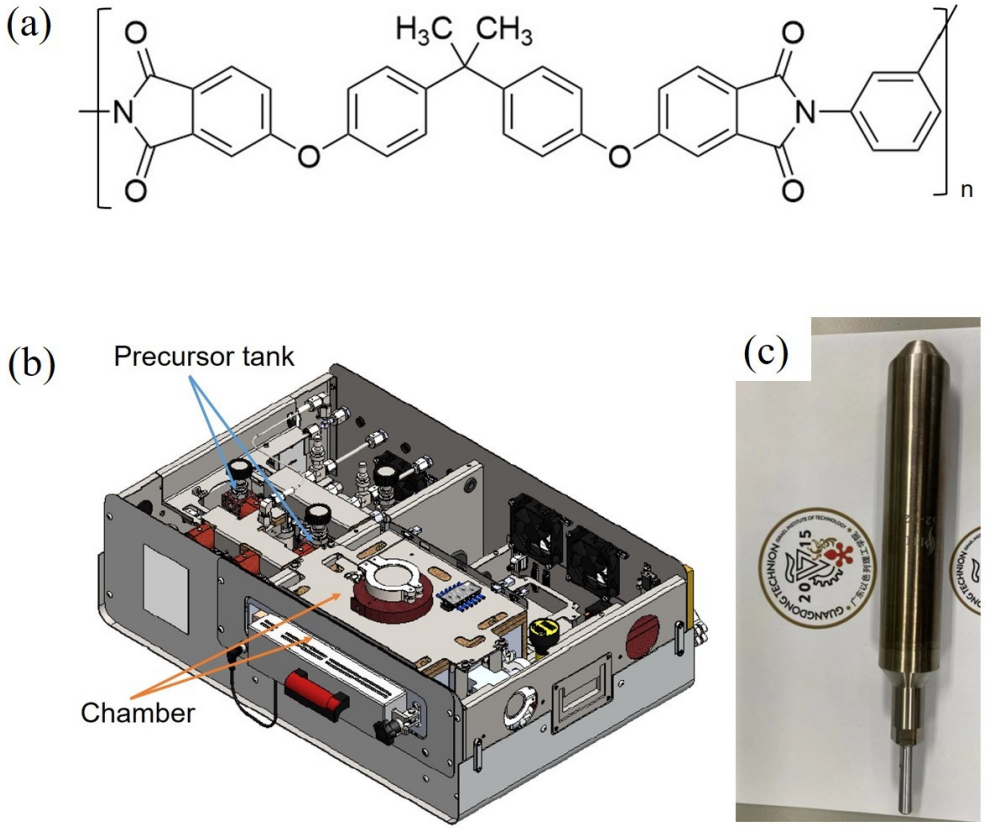

Figure S1. (a) The chemical structure of Polyetherimide (PEI). PEI is a modified version of PI and recyclable thermoplastic amorphous polymers with good solubility and processability.[1] (b) The ALD equipment. There are two storage tanks containing precursors respectively. The valves will be opened alternately, and then precursors are sent to the vacuum chamber by argon. (c) For better deposition, a small amount of 200mg of $BaTiO_3$ particles was put into the metal tool instead of the chamber in which the metal tool can rotate so that precursor molecules were adsorbed at any part of the core particles.

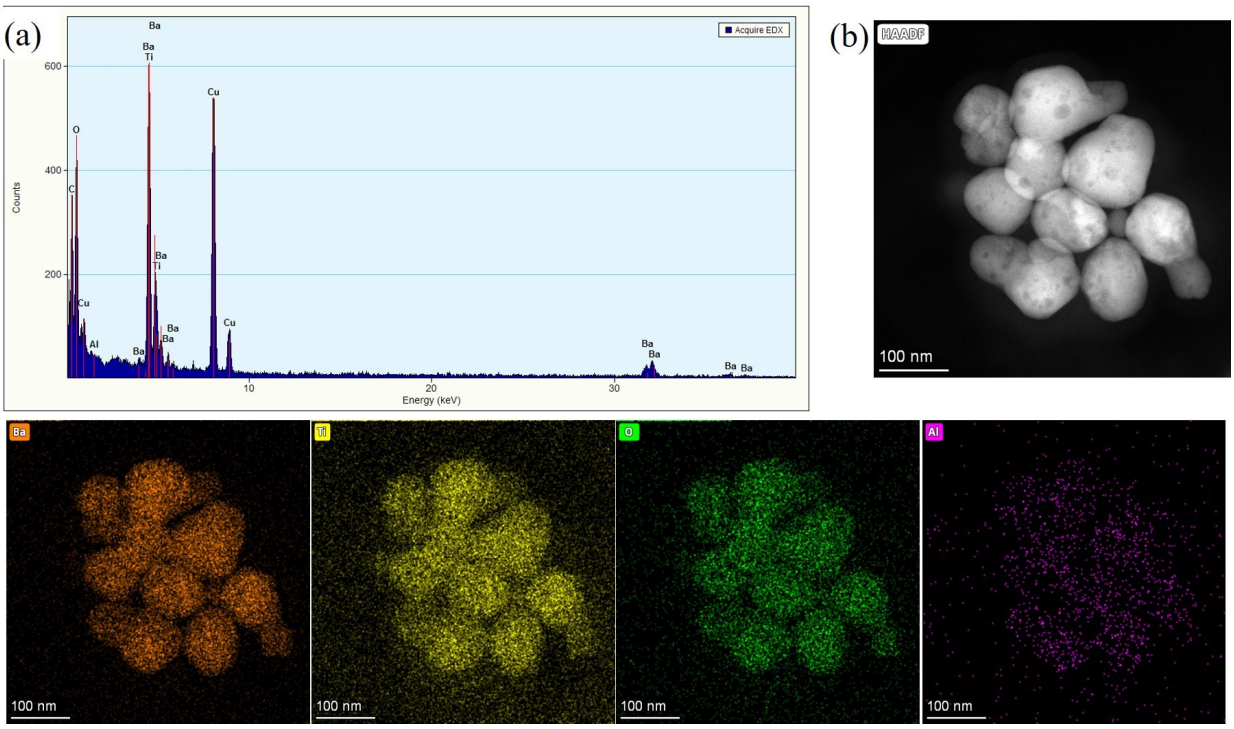

Figure S2. (a) The energy dispersive spectroscopy (EDS) shows the existence of all related elements. Copper should be neglected because the sample was put on the copper net. (b)The high-angle annular dark-field (HAADF) images and EDS with element mapping confirm the composition of $BaTiO_3@Al_2O_3$.

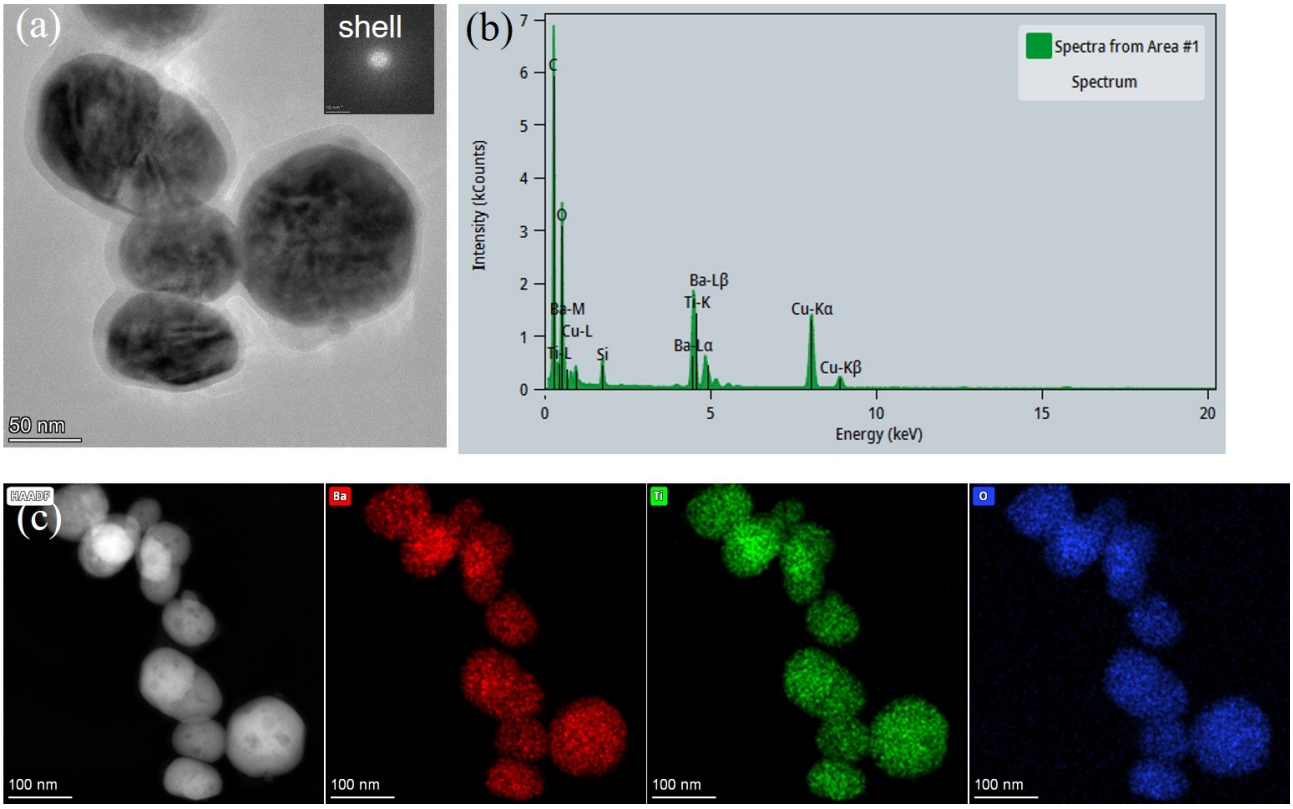

Figure S3. (a) TEM image of $BaTiO_3$@TiO_2. (b) The energy dispersive spectroscopy (EDS) shows the existence of all related elements. The Ti content is higher than Ba, implying the ALD contributed more Ti. (c) The HAADF images and EDS with element mapping confirm the composition of $BaTiO_3$@TiO_2.

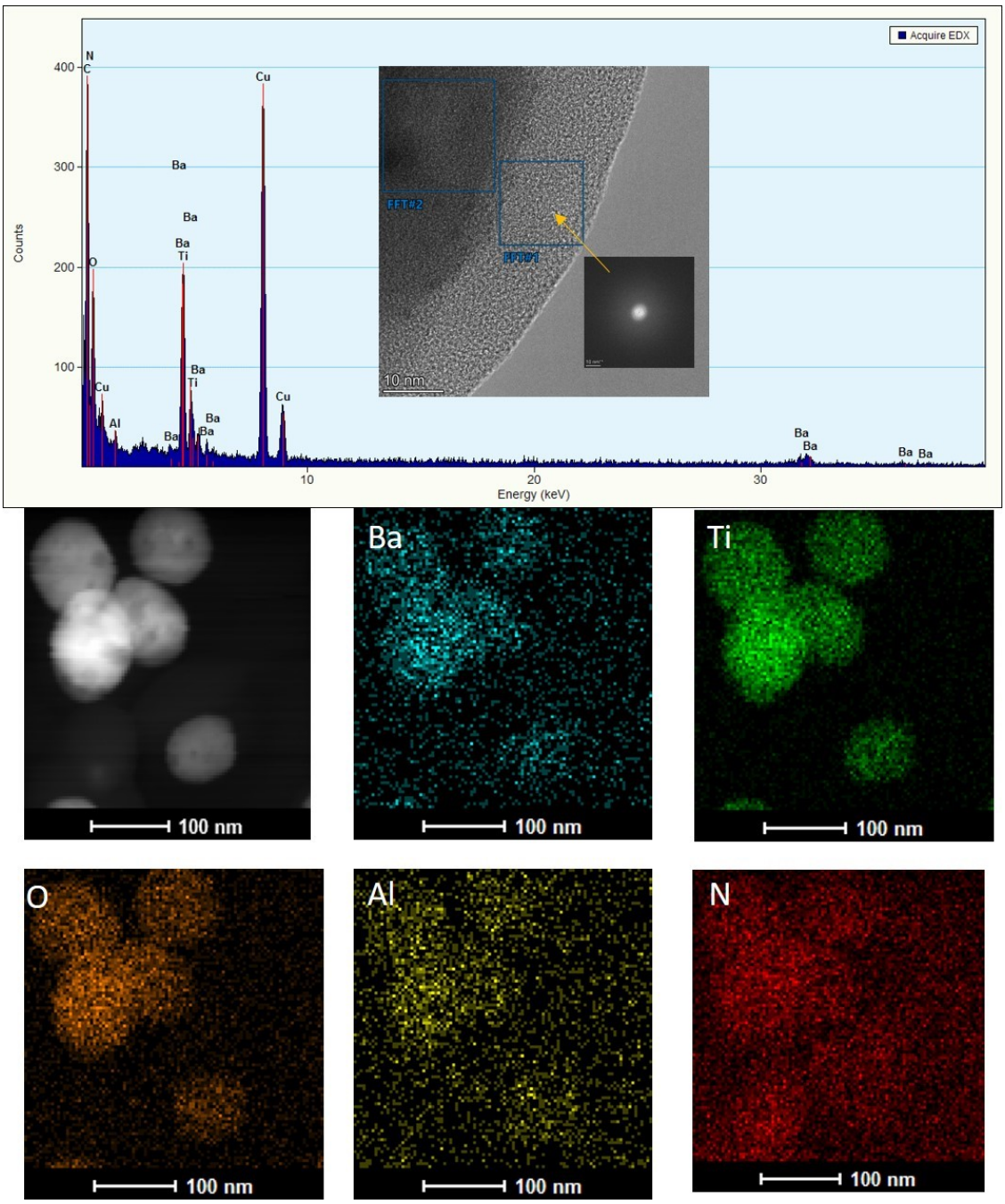

Figure S4. The EDS shows the existence of all related elements. The HAADF images and EDS with element mapping confirm the composition of $BaTiO_3$@AlN.

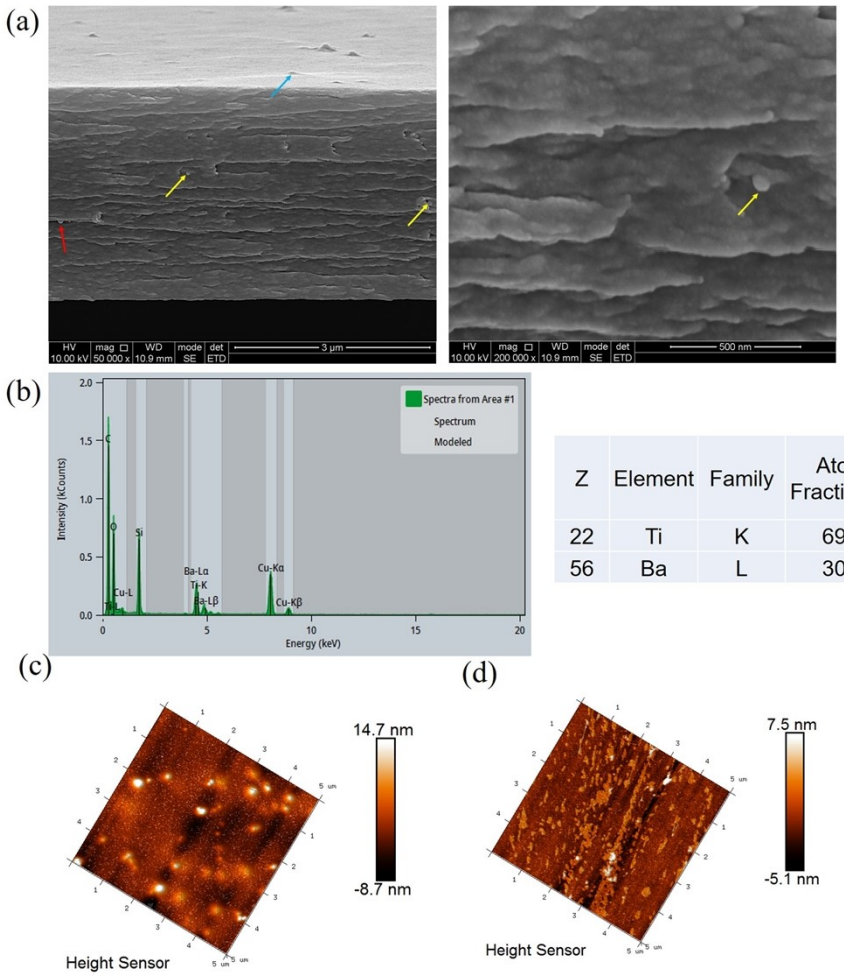

Z	Element	Family	Atomic Fraction (%)	Atomic Error (%)
22	Ti	K	69.88	6.84
56	Ba	L	30.12	4.35

Figure S5. (a) The cross-section SEM images of PEI/$BaTiO_3$@ TiO_2 film. It can be seen that the several exposed fillers in the polymer matrix. (b) The EDS of PEI/$BaTiO_3$@TiO_2 composite film, corresponding to Figure 2c. (c) The AFM image of 0.7 vol.% $BaTiO_3$@ TiO_2 film. Ra = 1.78 nm, Rq = 2.73 nm. (d) The AFM image of PEI. Ra = 1.22 nm, Rq = 1.79 nm.

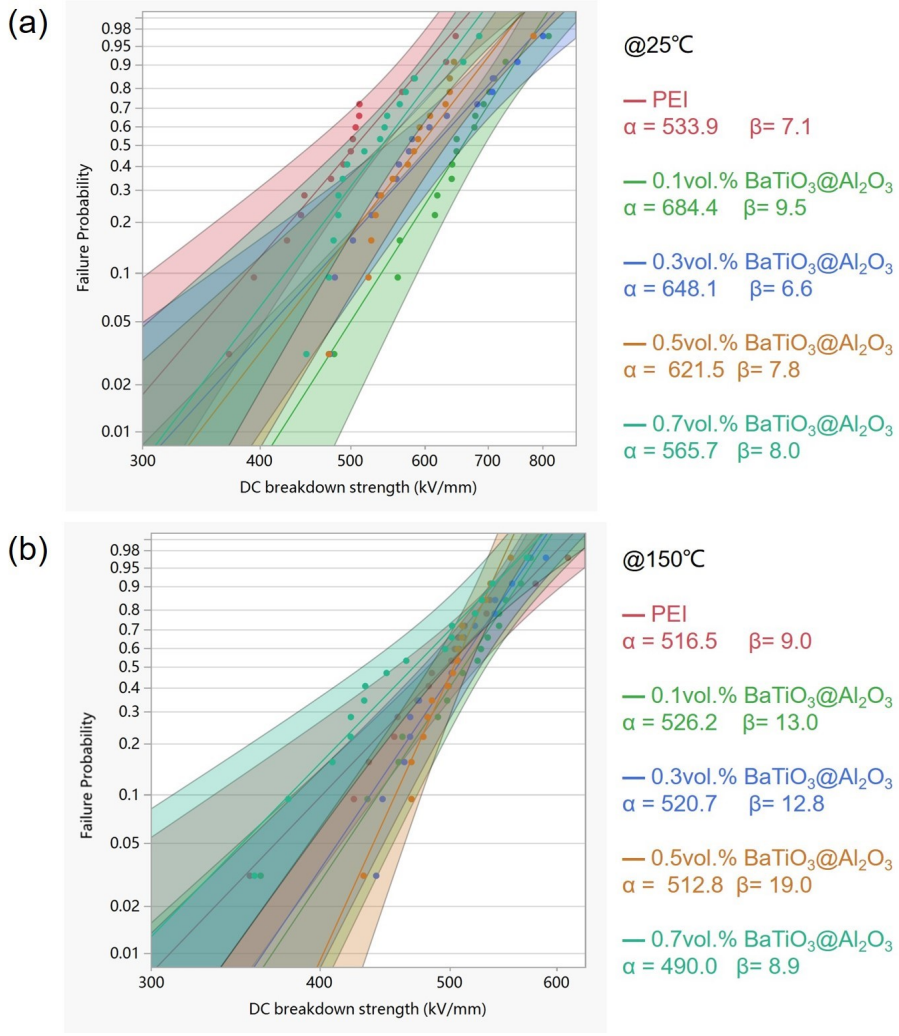

Figure S6. The breakdown strength used to be described by the Weibull distribution.[2] (a) The Weibull distribution curves of PEI and PEI/ $BaTiO_3@Al_2O_3$ composites films at room temperature and 150℃ (b). At room temperature, the breakdown strength of composites is higher than the PEI matrix no matter what filler content, which indicates the positive effects of the fillers. At 150℃, with the increment of filler content, the breakdown strength presents a slight reduction, but is still higher than PEI when the filler content is lower than 0.3vol.%.

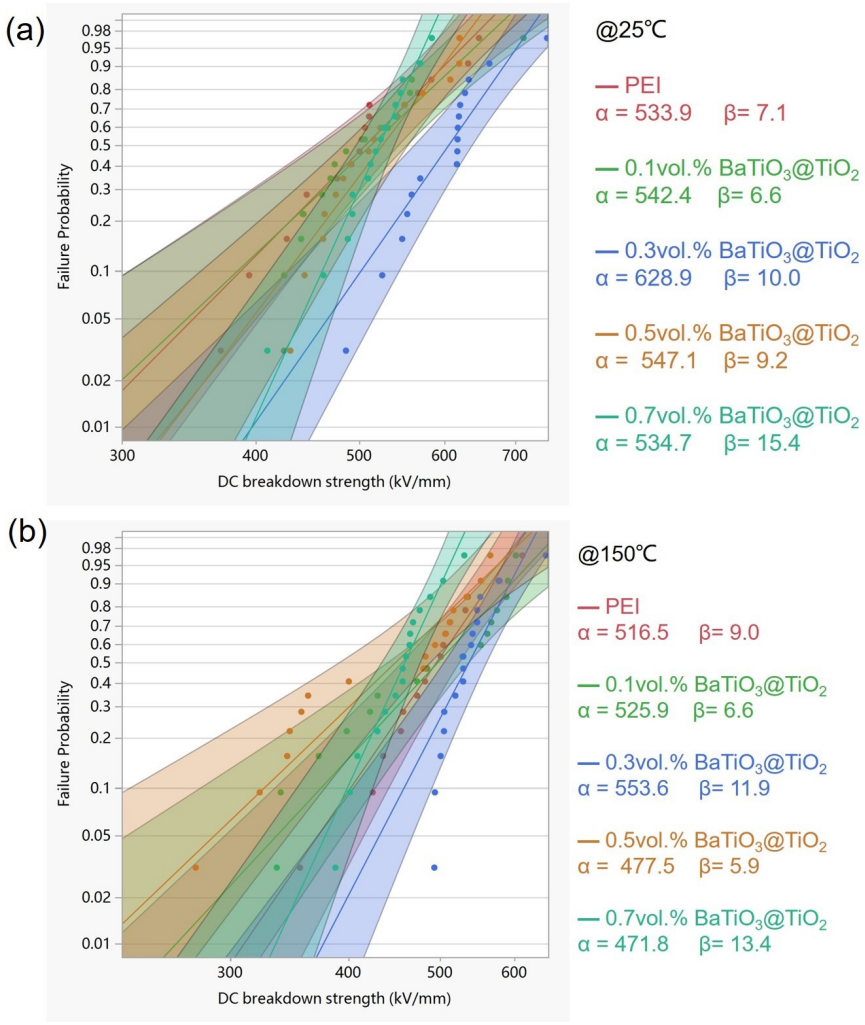

Figure S7. (a) The Weibull distribution curves of PEI and PEI/ $BaTiO_3$@TiO_2 composites at room temperature and 150℃ (b). At room temperature, the breakdown strength of composites is higher than the PEI matrix and reaches a maximum value when the filler is 0.3vol.%. At 150℃, the breakdown strength is higher than PEI when the filler content is lower than 0.3vol.%.

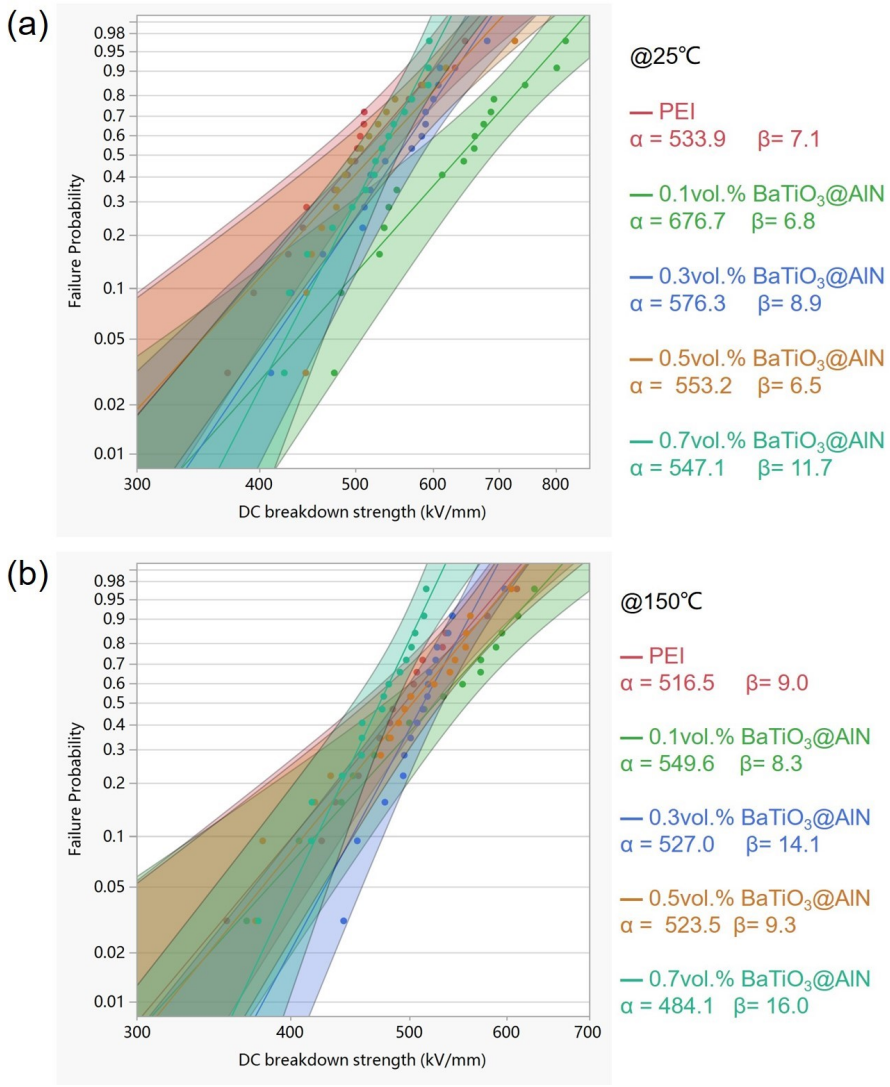

Figure S8. (a) The Weibull distribution curves of PEI and PEI/ $BaTiO_3$@AlN composites at room temperature and 150℃ (b). At room temperature, the breakdown strength of composites is higher than the PEI matrix and reaches a maximum value when the filler is 0.1vol.%. At 150℃, the breakdown strength is higher than PEI when the filler content is lower than 0.5vol.%.

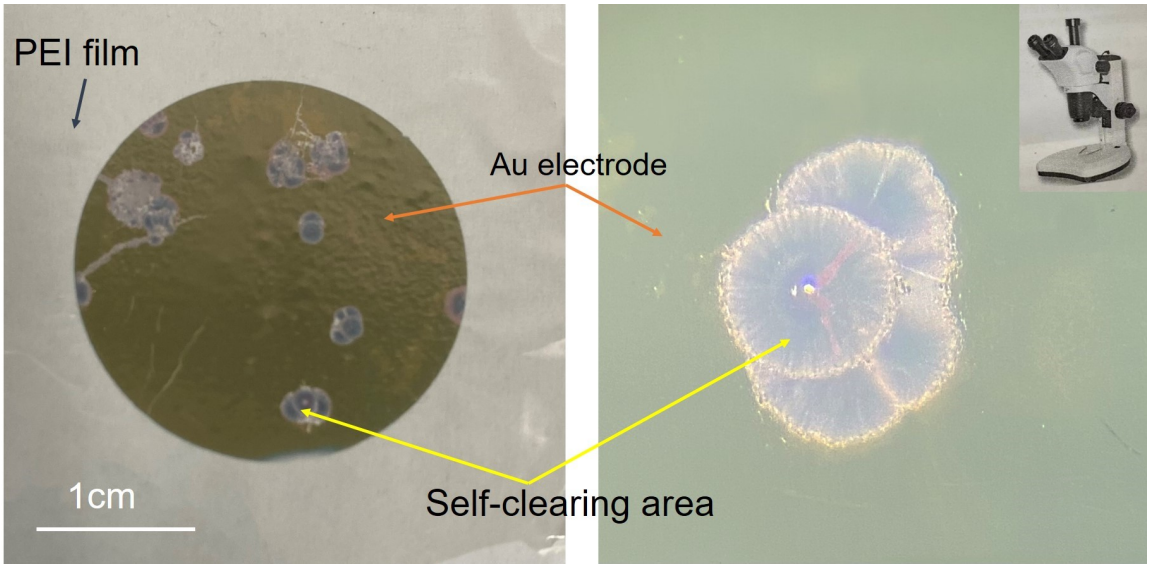

Figure S9. The self-clearing test is shown here. One side of the PEI film was sputtered with a gold electrode with a diameter of 25mm. Under a high voltage, Joule heat may lead to the vaporization of the metal electrode on the film surface.[3] Especially when the newly exposed surface area under the metal electrode is large enough to isolate the carbonized perforation, the self-clearing supports the capacitor's continued operation (right optical picture). The self-clearing process eliminated the weak points in the dielectric, improving the reliability of the capacitor.[4]

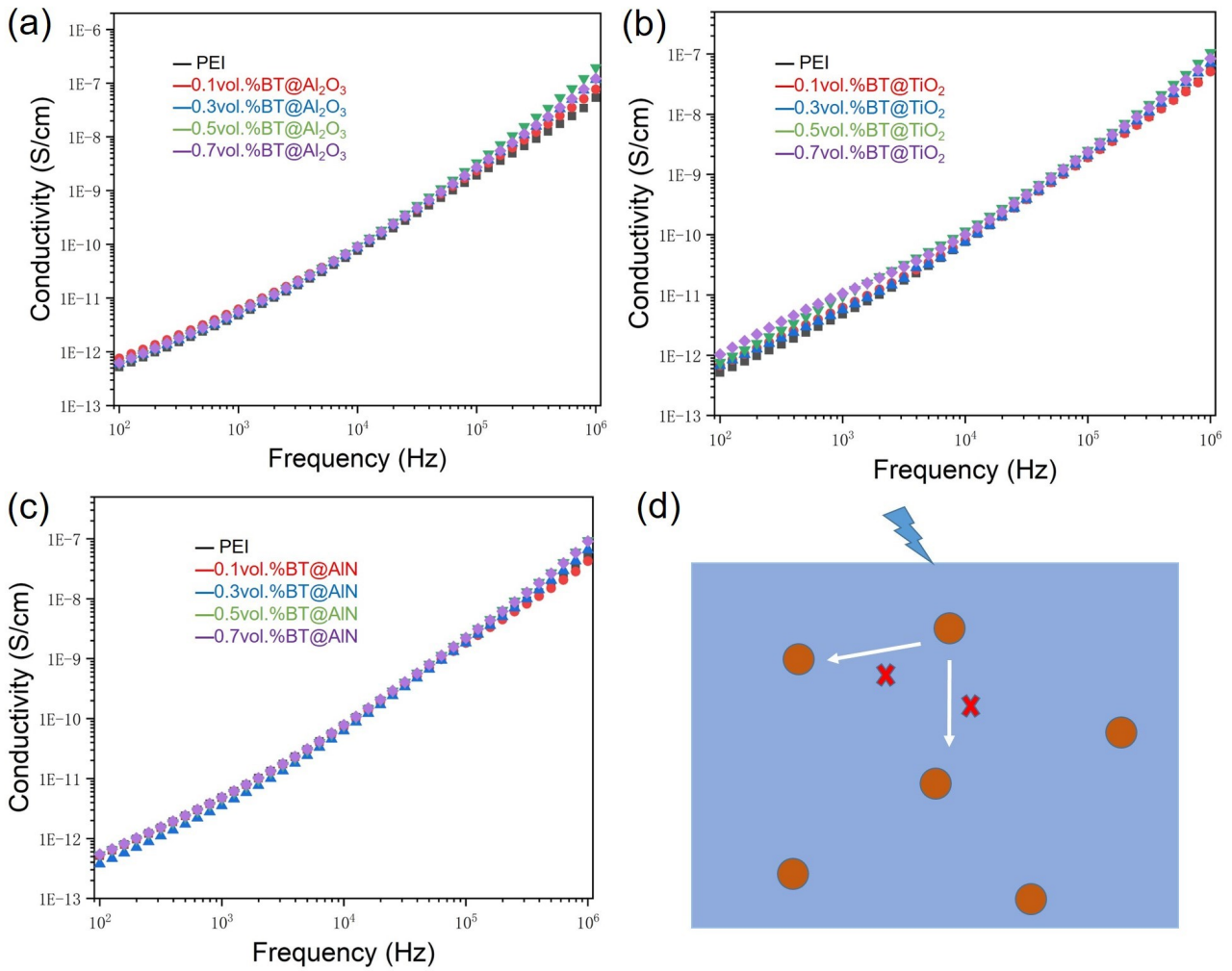

Figure S10. Alternating current conductivities of different films. The conductivity increases with the increment of frequency because at lower frequencies charge carriers are forced to migrate over larger distances and their transport is significantly restricted by the presence of isolated conductive sites, while at high frequencies localized charge carrier takes maximum advantage of conducting regions.[5] The extremely small difference in the curves indicates that the low content fillers cannot change the electrical insulation because it is difficult to form a conduction path in the polymer matrix.

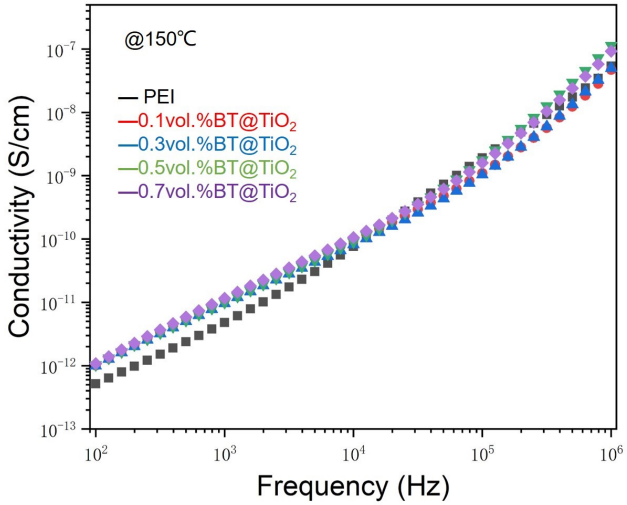

Figure S11. Alternating current conductivities of PEI and PEI/ $BaTiO_3$@TiO_2 films at 150℃. When the frequency is below 10^4 Hz, the conductivity increases compared with those at 25℃, and the influence of temperature is more pronounced at lower frequencies, revealing a thermally activated conduction mechanism. The influence of temperature decays with increasing frequency, and the conductivity values display proximity in the high-frequency range, appearing to be independent of temperature, which is consistent with the epoxy resin/$BaTiO_3$ system[5].

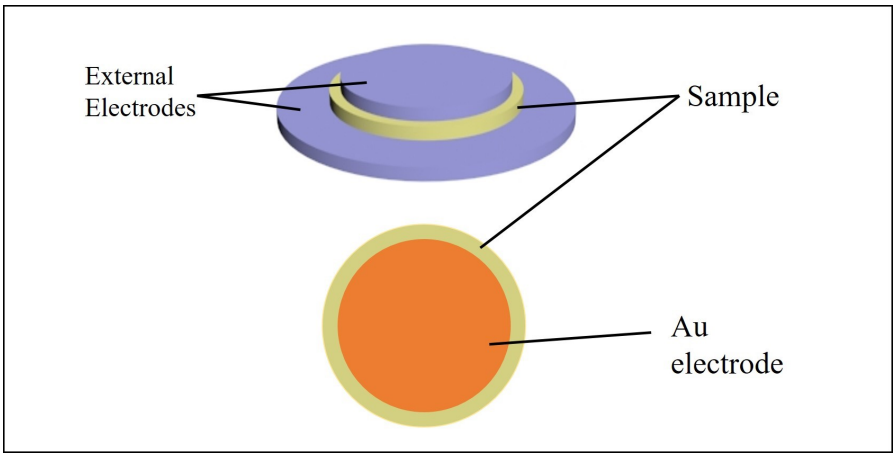

Figure S12. The diagram of the dielectric test. Two electrodes are used and samples with the gold electrode (~20nm thick and 20mm diameter) were sandwiched between the electrodes of clamps.[6]

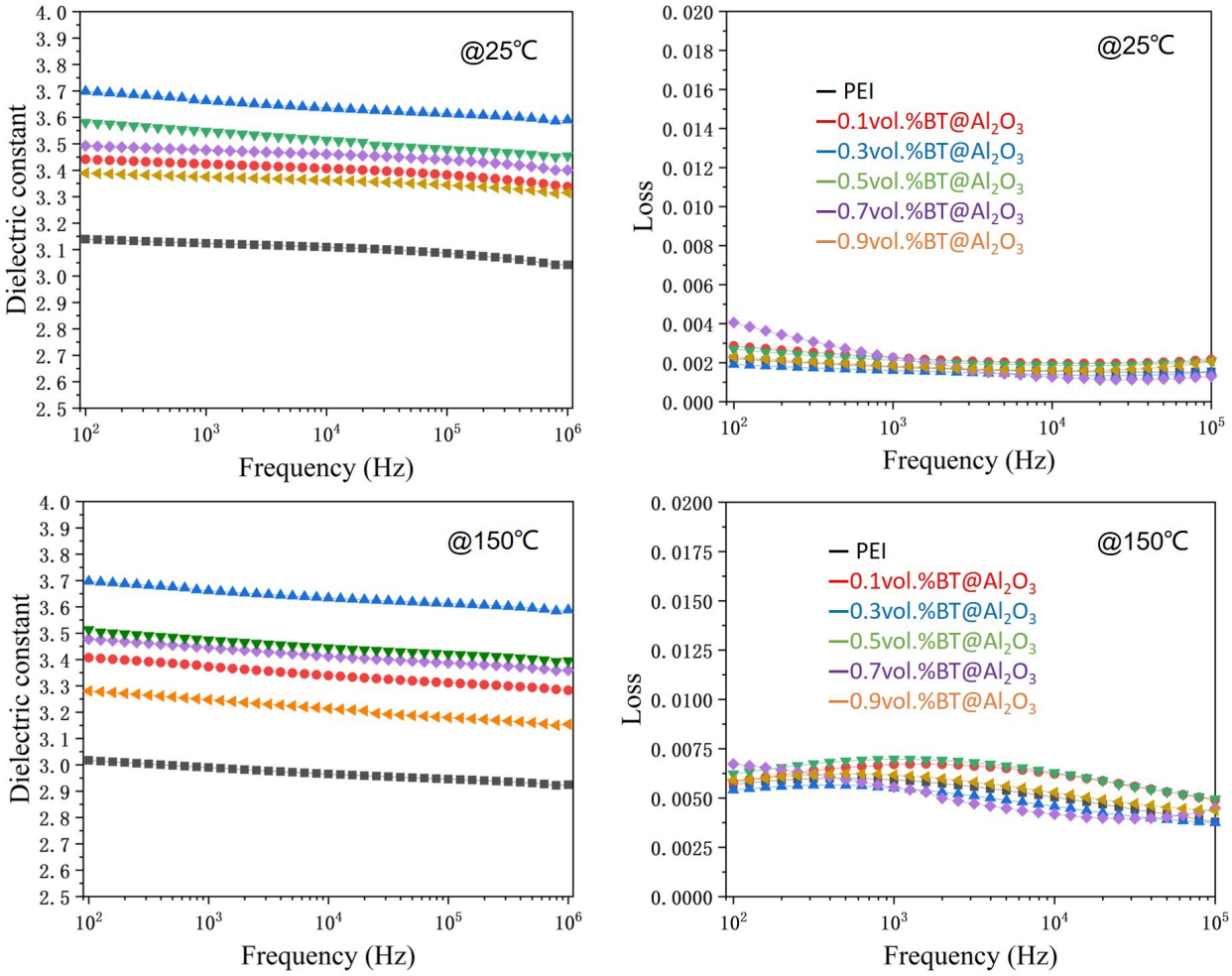

Figure S13. Dielectric constant and loss tangent of PEI and PEI/ $BaTiO_3$@Al_2O_3 films. With the addition of core-shell fillers, the dielectric constant increased and reached the maximum value when the filler is 0.3vol.%. The loss tangent still maintains the ultralow level (< 0.8%) even at 150℃ in the frequency from 100Hz to 10^5Hz.

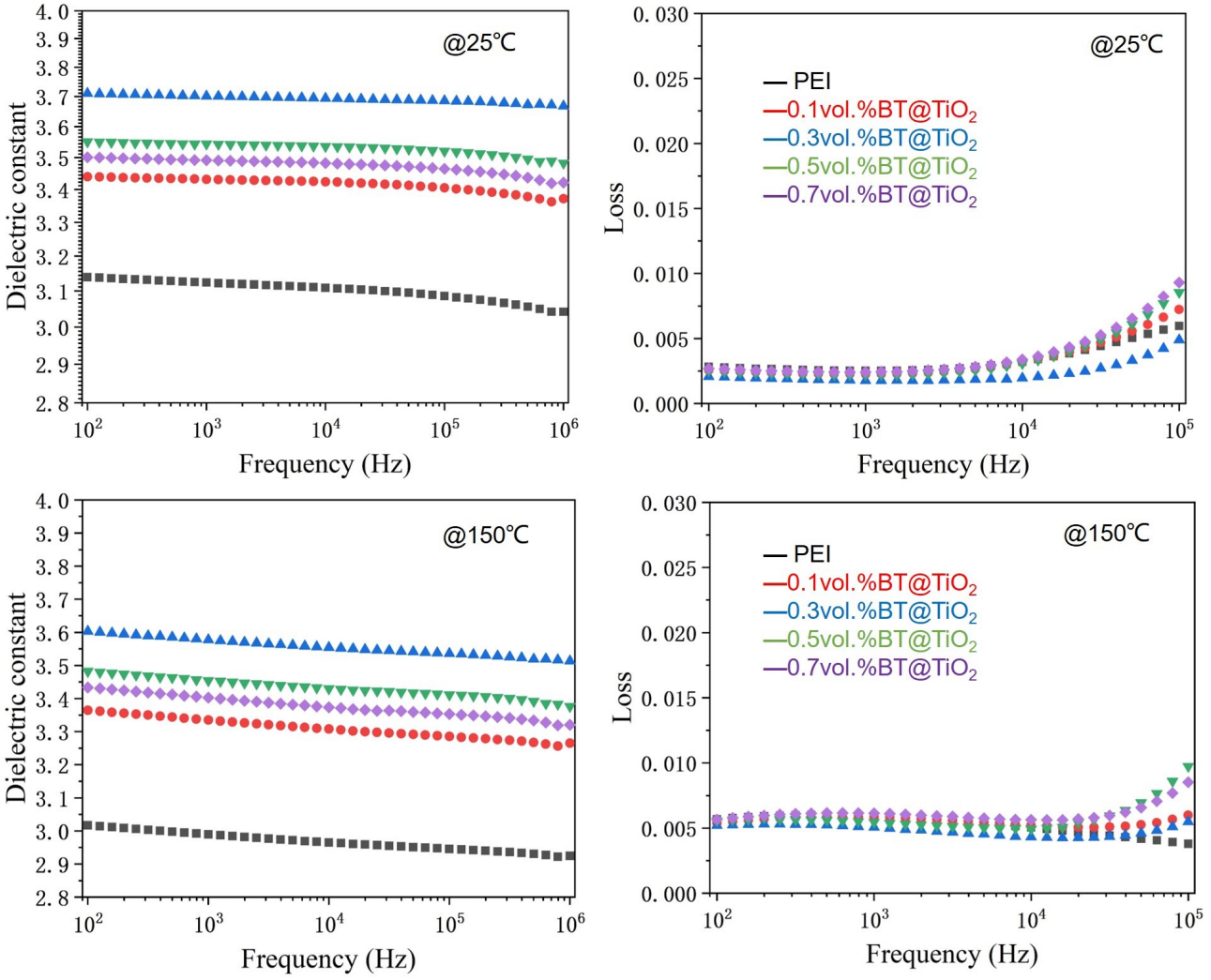

Figure S14. Dielectric constant and loss tangent of PEI and PEI/ $BaTiO_3$@TiO_2 films. With the addition of core-shell fillers, the dielectric constant increased and reached the maximum value when the filler is 0.3vol.%. The loss tangent still maintains a low level (< 1%) even at 150℃ in the frequency from 100Hz to 10^5Hz.

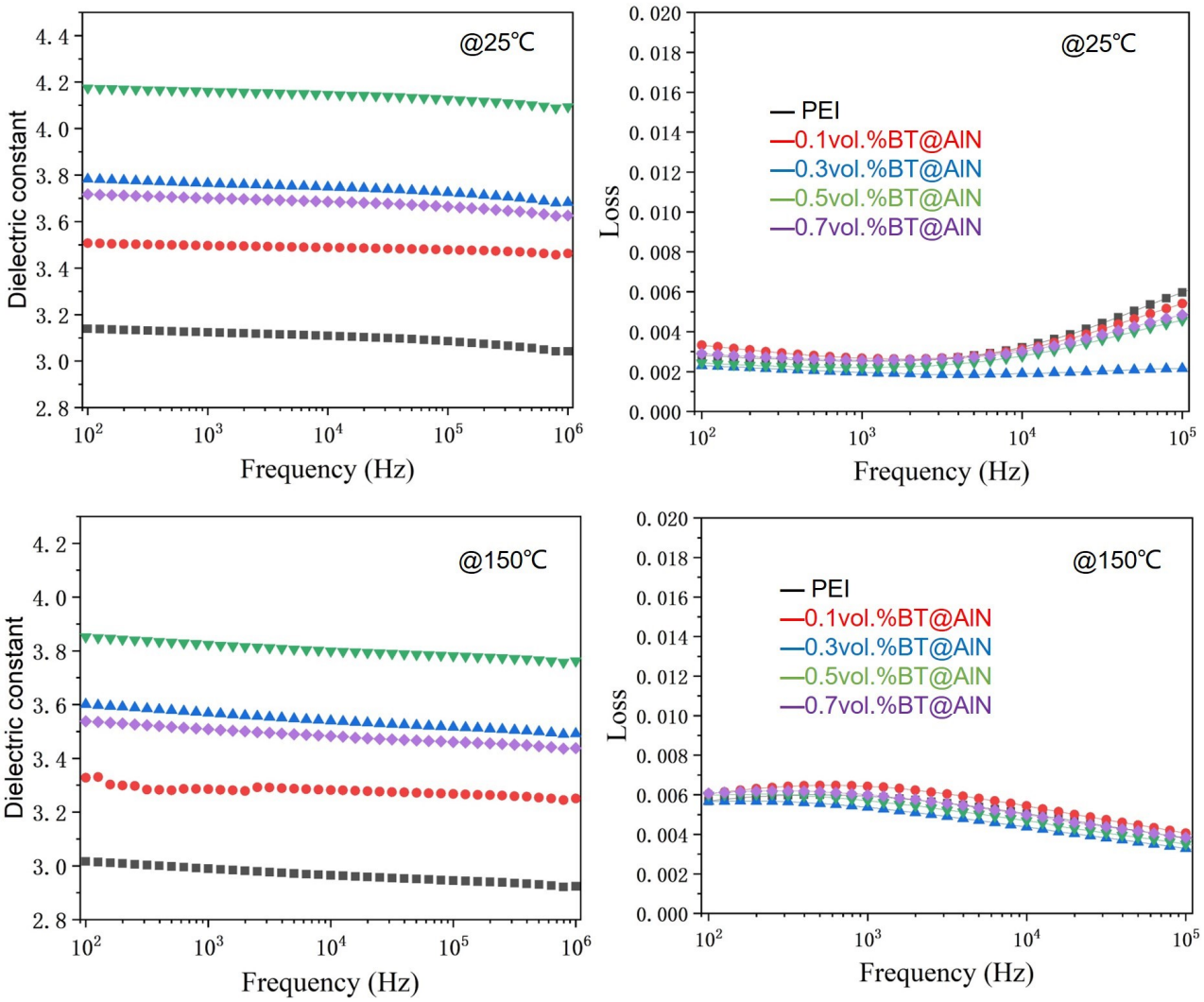

Figure S15. Dielectric constant and loss tangent of PEI and PEI/ $BaTiO_3$@AlN films. With the addition of core-shell fillers, the dielectric constant increased and reached the maximum value when the filler is 0.5vol.%. The loss tangent still maintains a low level (< 0.7%) even at 150℃ in the frequency from 100Hz to 10^5Hz.

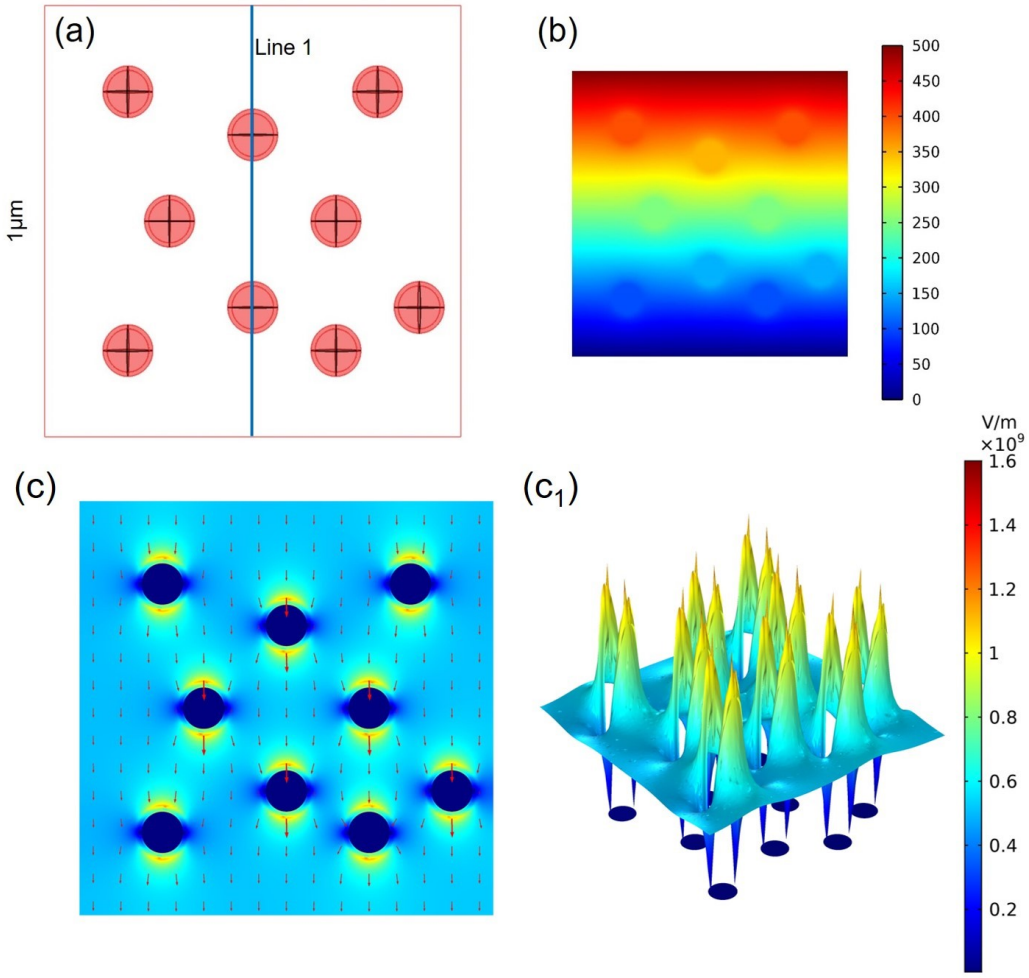

Figure S16. The finite element simulation of PEI / $BaTiO_3$@Al_2O_3 composites. (a) The 1μm x1μm plane of the simulation region. (b) The potential distribution of the plane. (c-c_1) Finite element simulation on electric field distribution PEI/$BaTiO_3$@Al_2O_3 composites with 20 nm shell thickness.

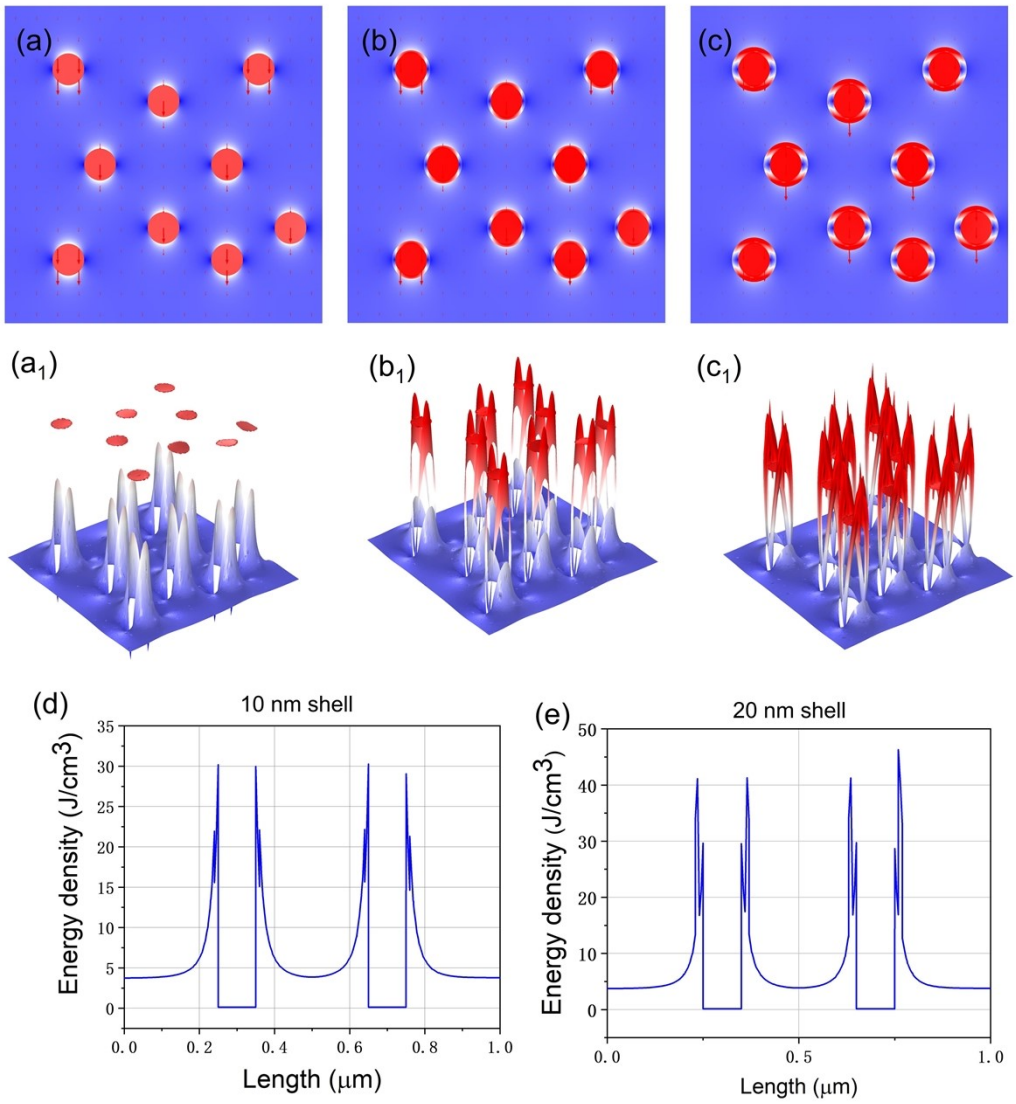

Figure S17. Finite element simulation on the polarization of PEI/$BaTiO_3$@Al_2O_3 composites with different shell thicknesses. (b) 10nm shell and (c) 20nm shell. (d-e) Computer-simulated energy density distribution of PEI-$BaTiO_3$@Al_2O_3 composite with 10nm and 20nm shell.

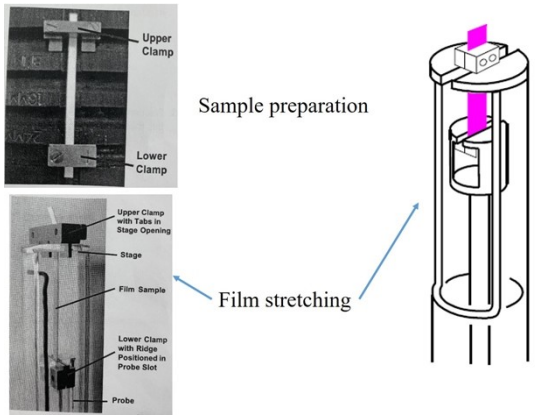

Figure S18. The diagram of the dimension change test. The tailored film was fixed in clamps and stretched under a constant extremely small external force.

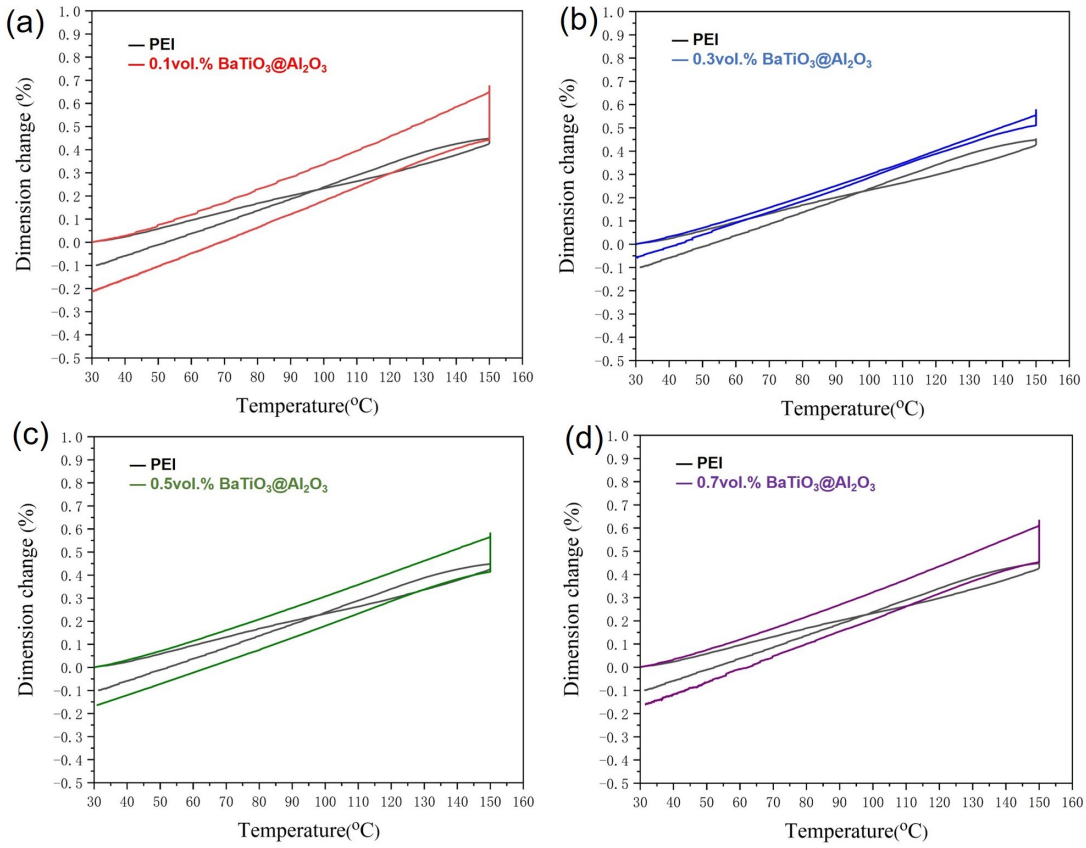

Figure S19. Deformation of PEI and PEI/ $BaTiO_3@Al_2O_3$ films from 30°C to 150°C and isothermal for 1h at 150°C. After one temperature cycle, all films maintain the small deformation of almost or less than 0.2%, such change does not influence capacitor application.

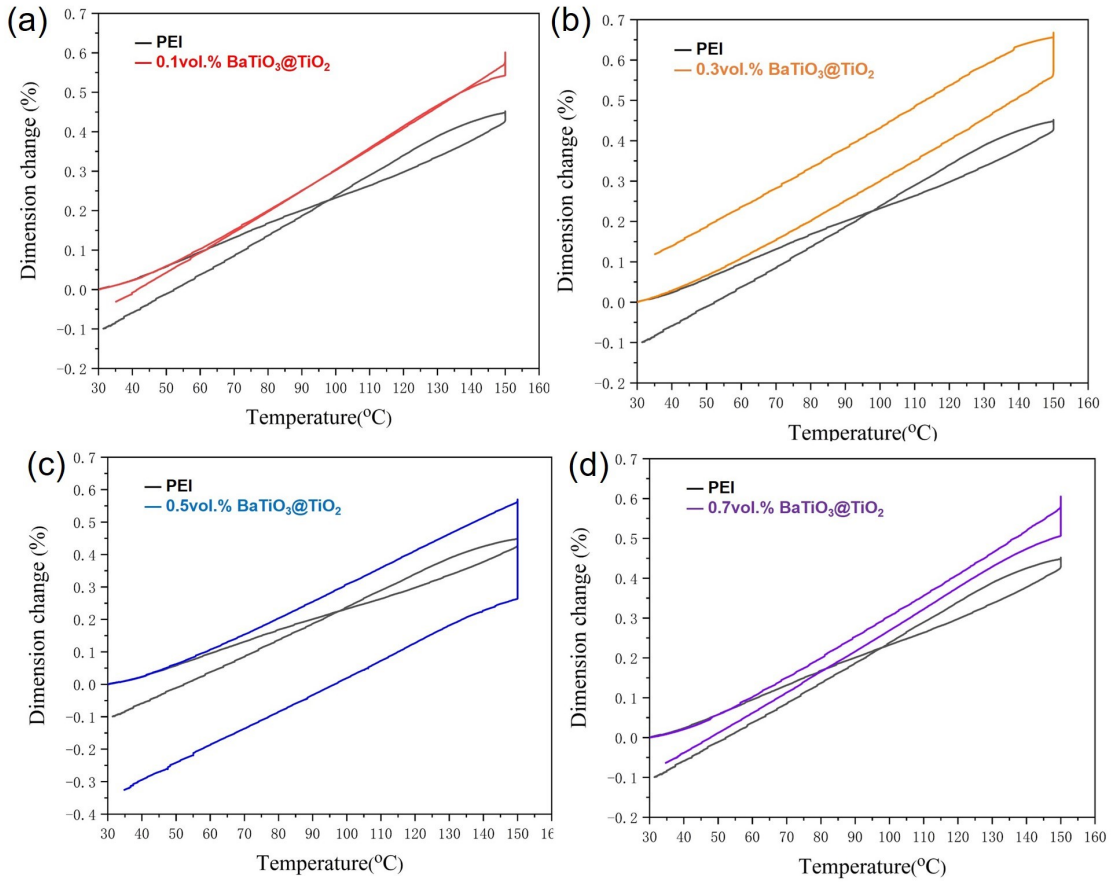

Figure S20. Deformation of PEI and PEI/ $BaTiO_3$@TiO_2 films from 30℃ to 150℃and isothermal for 1h at 150℃. After one temperature cycle, all films maintain the small deformation.

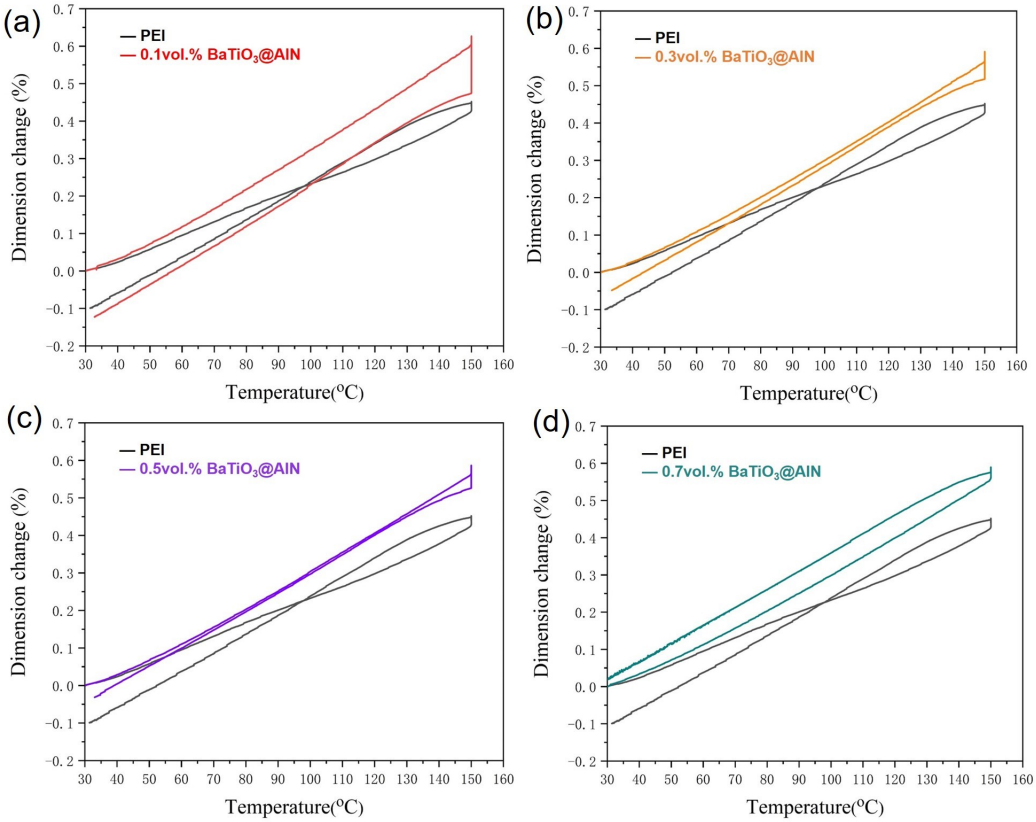

Figure S21. Deformation of PEI and PEI/ $BaTiO_3$@AlN films from 30℃ to 150℃and isothermal for 1h at 150℃. After one temperature cycle, all films maintain an extremely small deformation of about 0.1%.

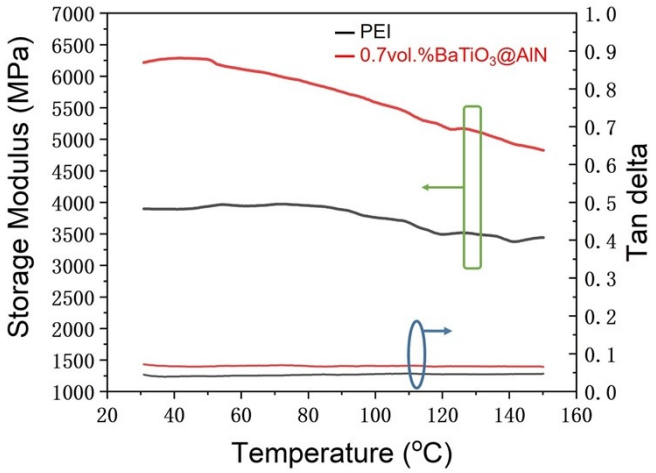

Figure S22. Dynamic mechanical analysis (DMA) of PEI and PEI / 0.7vol.% $BaTiO_3$@AlN films. The oscillation frequency was 1 Hz. The samples were heated at a rate of 5 °C/min from 30 to 150 °C. It should be noted that the higher storage modulus of PEI / 0.7vol.% $BaTiO_3$@AlN film does not mean higher Young's modulus because the different film thicknesses were tested.

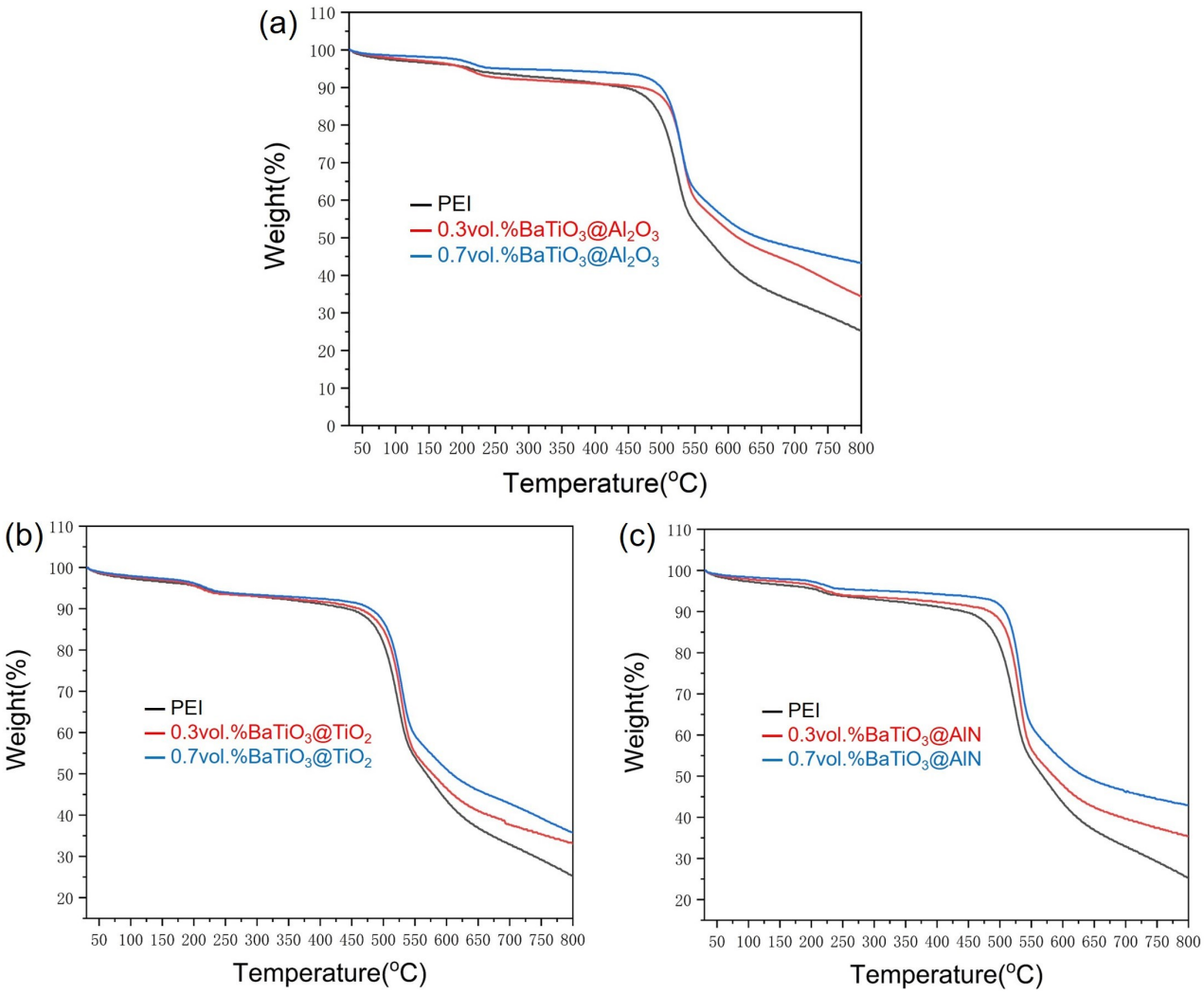

Figure S23. Thermal Gravimetric Analyzer (TGA) curves of PEI and composites films. The first step is related to the decomposition of the non-aromatic part of PEI (~523℃) and the second one to the decomposition of the aromatic part.[7] At 800℃, more residue in higher filler composites films indicates the homogeneous distribution of fillers.

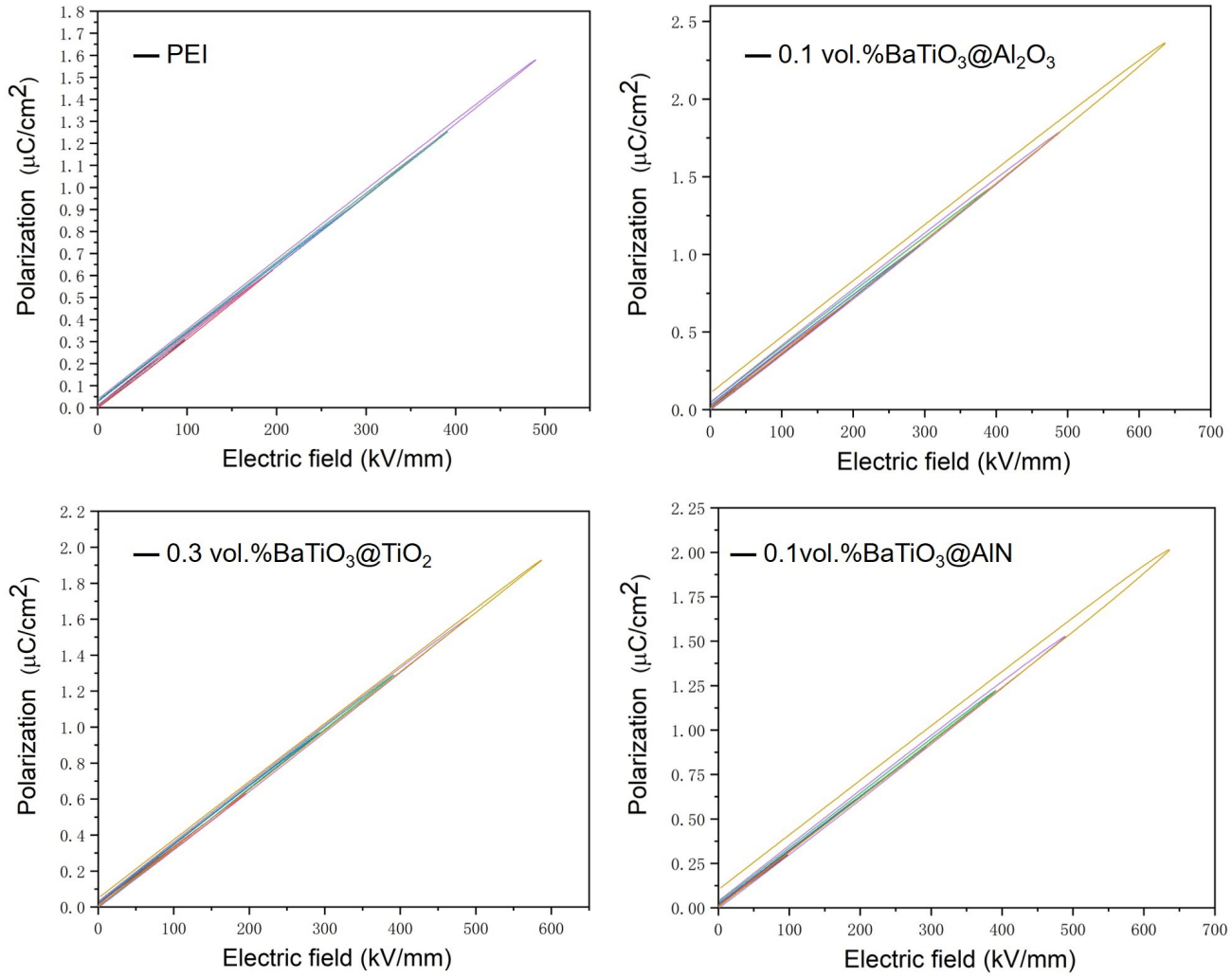

Figure S24. The energy density and discharge energy density can be calculated from the polarization–electric field curves (P-E loops).[8]

Table S1. The property summary of PEI / core-shell composites

Polymer/ composites	Filler volume (%)	Electric strength (V/μm)	Discharged energy density(J/cm^3)	Efficiency (%)
PEI	0	500	3.74	96.9
PEI / $BaTiO_3$@Al_2O_3	0.1	650	7.06	93.0
	0.3	600	5.44	95.9
	0.5	550	4.72	94.3
	0.7	500	3.95	93.4
PEI / $BaTiO_3$@TiO_2	0.1	500	3.82	96.7
	0.3	600	5.47	96.6
	0.5	500	4.21	94.6
	0.7	500	4.62	87.9
PEI / $BaTiO_3$@AlN	0.1	650	5.97	92.1
	0.3	550	4.44	91.5
	0.5	500	4.17	89.1
	0.7	500	4.38	88.4

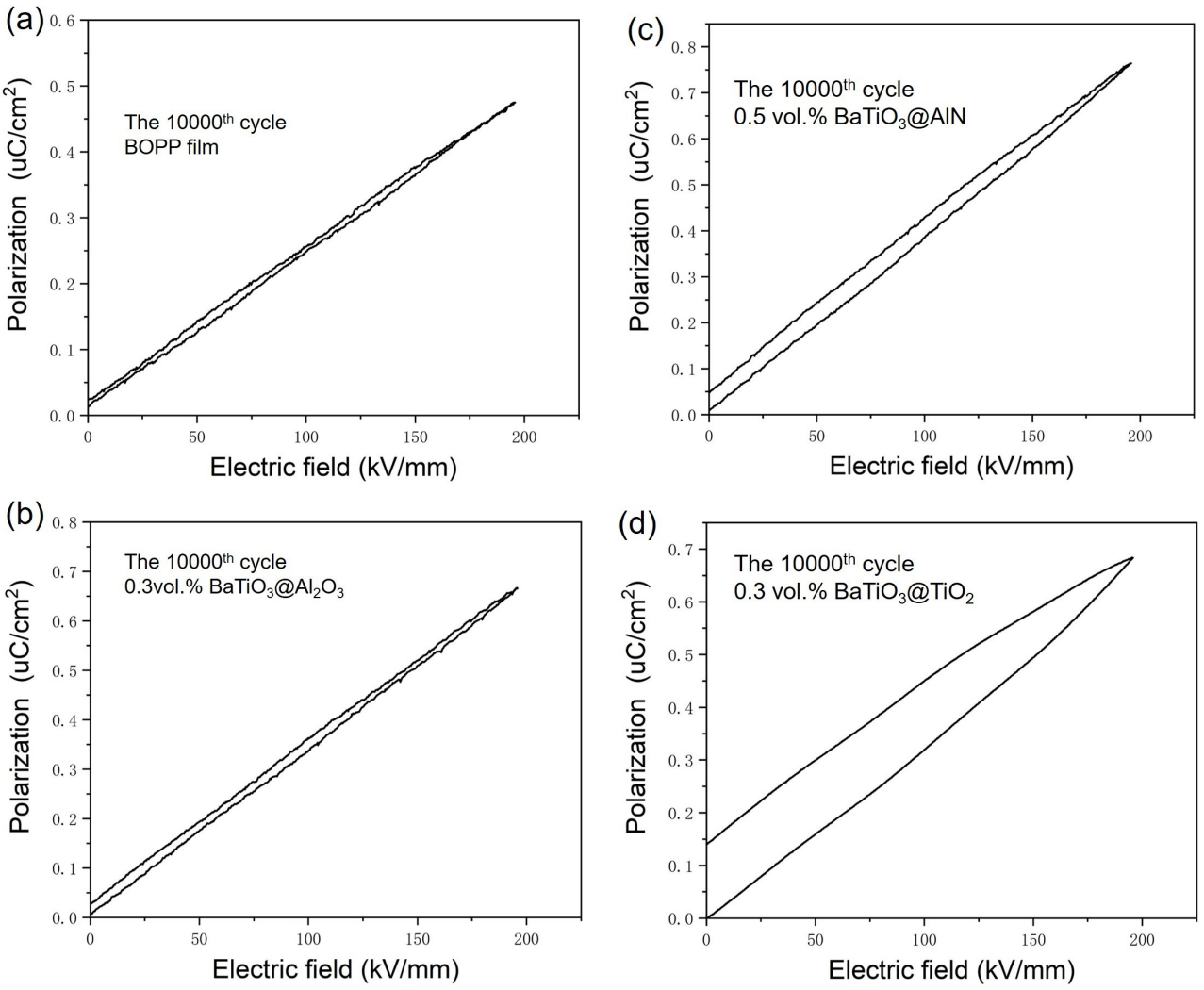

Figure S25. Fatigue test of BOPP film and PEI / core-shell fillers composite film. From the curve, we can see that the polarization strength of the composite film is higher than BOPP even at the 10000th cycle.

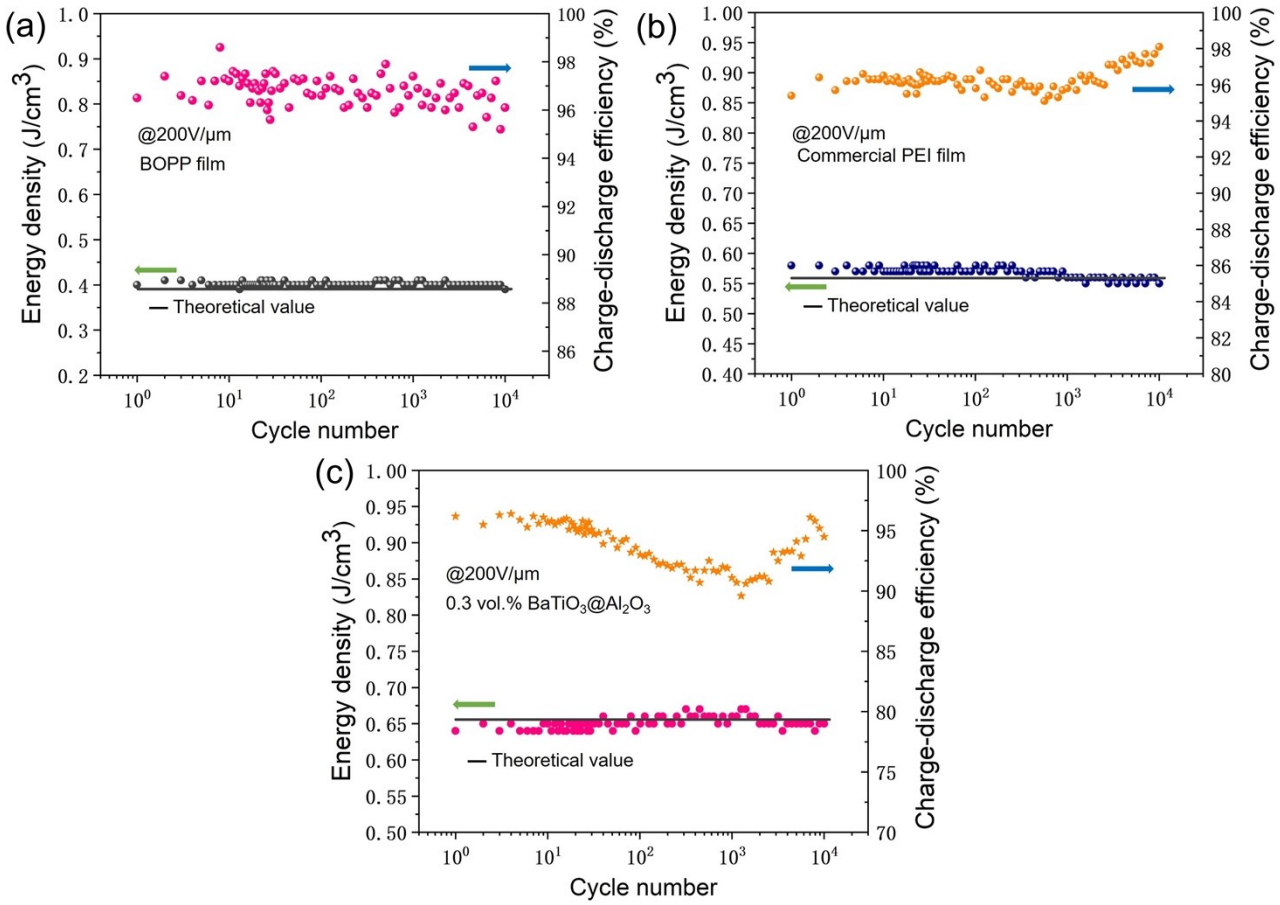

Figure S26. (a-c) The cycle stability of commercial BOPP and PEI, and PEI/$BaTiO_3$@Al_2O_3 composites films.

[1] R. O. Johnson, H. S. Burlhis, "Polyetherimide: A new high-performance thermoplastic resin", presented at *J. Polym. Sci., Polym. Symp.* 1983.

[2] W. Weibull, *J. Appl. Mech.* 1951,**18**,293.

[3] Y. Zhang, H. Khanbareh, J. Roscow, M. Pan, C. Bowen, C. Wan, *Matter* 2020,**3**,989.

[4] X. Wu, X. Chen, Q. Zhang, D. Q. Tan, *Energy Storage Mater.* 2022,**44**,29.

[5] G. Psarras, in *Physical properties and applications of polymer nanocomposites*, Elsevier, 2010, 31.

[6] X. Wu, J. Huang, S. Yu, P. Ruan, R. Sun, C.-P. Wong, *Macromol. Res.* 2020,**28**,373.

[7] H. Abbasi, M. Antunes, J. Velasco, *Express Polym. Lett*. 2015,**9**.

[8] T. M. Chung, *Green Sustainable Chem*. 2012,**2**,29.